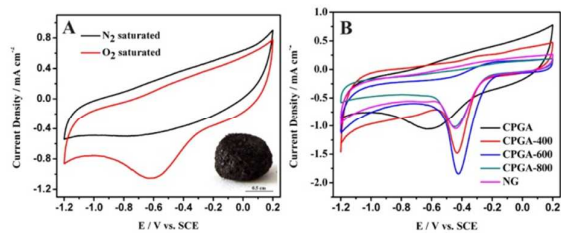




Design and synthesis of carbonized polypyrrole coated graphene aerogel act as an efficient metal-free catalyst for oxygen reduction

Journal:	<i>RSC Advances</i>
Manuscript ID:	RA-ART-01-2014-000015.R1
Article Type:	Paper
Date Submitted by the Author:	10-Mar-2014
Complete List of Authors:	Wei, Hua; Key Laboratory of Material and Technology for Clean Energy, Ministry of Education, Key Laboratory of Advanced Functional Materials, Institute of Applied Chemistry, Xinjiang University, Xu, Mao-Wen; Institute of Clean Energy & Advanced Materials, Southwest University, Chongqing, BAO, SHU-JUAN; Institute for Clean Energy & Advanced Materials, Yang, Fan; Key Laboratory of Material and Technology for Clean Energy, Ministry of Education, Key Laboratory of Advanced Functional Materials, Institute of Applied Chemistry, Xinjiang University, Chai, Hui; Key Laboratory of Material and Technology for Clean Energy, Ministry of Education, Key Laboratory of Advanced Functional Materials, Institute of Applied Chemistry, Xinjiang University,



Synthesis 3D N-doped graphene aerogel for ORR in alkaline electrolyte under hydrothermal process without any oxidant.

Cite this: DOI: 10.1039/c0xx00000x

www.rsc.org/xxxxxx

ARTICLE TYPE

Design and synthesis of carbonized polypyrrole coated graphene aerogel act as an efficient metal-free catalyst for oxygen reduction

Hua Wei^a, Mao-Wen Xu^b, Shu-Juan Bao^{a,b*}, Fan Yang^a, Hui Chai^a

⁵ Received (in XXX, XXX) Xth XXXXXXXXX 20XX, Accepted Xth XXXXXXXXX 20XX

DOI: 10.1039/b000000x

Carbonized polypyrrole (PPy) coated graphene aerogel (CPGA) was synthesized by using graphene oxide and fresh pyrrole (Py) as raw materials under hydrothermal process without any oxidant. After annealing at high temperature, the as-prepared aerogel has a porous 3D network, contains a high percentage of nitrogen, and delivers a promising electrochemical catalytic activity. Most importantly, the annealing temperature has a significantly impact on the electrochemical performance of the obtained materials. Among of these products, after sintering at 600 °C, the as-prepared sample (CPGA-600) displays the most positive onset potential and highest peak current density for oxygen reduction reaction (ORR). The electrocatalytic mechanism of the as-prepared materials for ORR in alkaline electrolyte was also analyzed in detail. The results indicated that pyrrolic-N and highly graphitized carbon structures are mainly responsible for the enhanced ORR activity of metal-free N doped carbon materials.

15 •

1. Introduction

The oxygen reduction reaction (ORR) is one of the most important reactions in energy conversion systems such as metal-air batteries and fuel cells¹⁻². Platinum-based materials play a crucial role as exclusive catalysts for ORR for a long-time³. However, the high cost, limited supply, and weak durability of platinum catalysts hinder the large-scale industrial applications of fuel cells⁴. Therefore, the search for non-precious metal as well as metal-free catalysts for ORR is one of the most active and competitive field in material and chemistry⁵. Currently researches indicated that the heteroatom-doped carbon nanomaterial (nitrogen, boron and sulfur) can tailor their electronic property and chemical reactivity, as well as give rise to new functions, which were regarded to be a class of promising non-precious electrocatalysts towards ORR⁶⁻⁸. Recent reports demonstrated that nitrogen-doped graphene (NG) shows excellent electrocatalytic activity toward ORR, which reveals the possibility to replace expensive platinum-based catalysts with nitrogen-doped carbon materials and encourages us to look for highly efficient metal-free catalysts⁹⁻¹⁰.

Furthermore, the electrocatalytic activity of N-doped graphene is also affected by its microstructure, surface area and pore distribution, and so on. Three-dimensional (3D) graphene-based frameworks, such as hydrogels, aerogels, macroporous foams are new-generation porous carbon materials, which exhibit continuously interconnected porous structures, large surface area, and high electrical conductivity¹¹⁻¹⁴. Graphene aerogel is an ideal prototype for the maximization of accessible surface areas and development of high-performance electromechanical devices¹⁵⁻¹⁶. The catalysts based on 3D graphene architectures have unique

structure and properties. Their interconnected porous network and conductive multiplexed pathways are beneficial to rapid ion diffusion and charge transfer and provides special reaction microenvironment¹⁷. The rich joints and greatly overlap of graphene sheets are helpful to increase the electrical conduction. Hence, 3D graphene aerogel with much stacking of graphene sheets would be an optimal choice.

Here, we report an easy self-assembly approach to synthesis carbonized PPy coated graphene aerogel by a facile one-pot hydrothermal method. The obtained materials are furthermore pyrolysed at high temperature to form N-doped garphene aerogels, which have highly porous interconnected network, conductive multiplexed channels and high pyrrolic nitrogen content. As ORR catalysts, the as-synthesized N-doped garphene aerogel delivered superior performance for ORR, which may be due to the following reasons: The holey surface structure is created on individual graphene sheets to engender more exposed active edge sites; Nitrogen doping also improves the catalytic reactivity, while the formation of 3D porous structures significantly reduces graphene sheets stacking and facilitates fast transport of reactants/electrolytes.

2. Experimental Section

2.1 Synthesis of carbonized polypyrrole coated graphene aerogel (CPGA)

Grapheme oxide (GO) was prepared from natural graphite flakes using a modified Hummers method¹⁸⁻¹⁹. CPGA was prepared by hydrothermal assisted pyrolysis method as following. 10 mL GO (2 mg L⁻¹) aqueous solution with 1 mL fresh pyrrole

(Py) monomer was sonicated for 10 min, then the obtained stable suspension was adjusted to pH = 4 by 1 M hydrochloric acid. Subsequently, the suspension was sealed in a Teflon-lined autoclave and kept at 180 °C for 16 h. After that the as-prepared aerogel was freeze-dried for 24 h and further sintering at different temperature (400, 600 and 800 °C) for 2 h in Ar gas. The resultant samples are denoted as CPGA, CPGA-400, PGA-600 and CPGA-800, respectively.

For comparing, N-doped graphene (NG) was also prepared by conventional pyrolysis method, GO and Py with same mass ratio with above experiment were ground together in a mortar using pestle and the mixture was then pyrolysed at 600 °C for 2 h with a flow of Ar.

2.2 Fabrication of modified electrodes

For electrode preparation, 2 mg CPGA (CPGA-400, CPGA-600 and CPGA-800) was dispersed in 1 ml ethanol-water solution (volume ratio of ethanol to water is 1:1) for 0.5 h under sonication. And then 10 μL CPGA (CPGA-400, CPGA-600 and CPGA-800) was slightly dropped onto the disk surface of the pre-polished glassy carbon electrode. After solvent evaporation, the deposited catalyst was covered with 5 μL Nafion solutions (0.5% in ethanol) to fix the catalyst on the GCE surface and the prepared electrodes were allowed to dry in air. A glass carbon RDE (Autolab) after loading the electrocatalyst was used as the working electrode, saturated calomel electrode (SCE) as the reference electrode, and a Pt wire as the counter electrode. The electrochemical experiments were conducted in O₂-saturated 0.1 M KOH electrolyte for the oxygen reduction reaction. The potential range is cyclically scanned between -1.2 and +0.2 V at a scan rate of 50 mV s⁻¹ at the room temperature after purging O₂ or N₂ for 15 min. RDE measurements were conducted at different rotating speeds from 225 to 2500 rpm, using an Autolab Model, and RRDE measurements were carried out at 1600 rpm with an Autolab Model.

2.3 Materials characterization

The microstructure and morphology of the as-prepared samples were characterized by field-emission scanning electron microscopy (SEM, JSM-6700F) and high-resolution transmission electron microscopy (HRTEM, JEM-2100, Japan). The Raman spectrum (Bruker Senterra R200-L) was used to study the integrity and electronic structure of the samples. X-ray diffraction (XRD) analysis was performed on Bruker D8-ADVANCE diffractometer with Cu K α radiation at a wavelength of $\lambda=0.15418$ nm. X-ray photoelectron spectroscopy (XPS) data were acquired with a Kratos AXIS 165 Multitechnique Electron Spectrometer (Manchester, UK).

3. Results and discussion

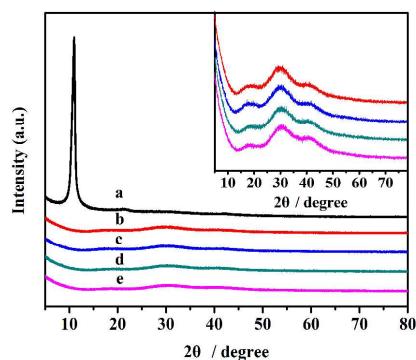


Fig. 1 XRD of as-prepared samples (a, GO; b, CPGA; c, CPGA-400; d, CPGA-600; e, CPGA-800)

Fig. 1 displays the XRD patterns of GO and as-prepared materials. The diffraction peak of GO appears at 10.9°, corresponding to its layered structure with an interlayer spacing of 8.12 Å²⁰. The XRD pattern of CPGA shows three broad diffraction peaks around 18.8 °, 29.7 ° and 40.8 °. Comparing with GO, for the resulting CPGAs, the peak at 10.9° disappeared and no obvious peaks for pristine graphite are observed in the XRD pattern, which confirmed the GO had been fully converted into the graphene structure during hydrothermal treatment and annealing process²¹.

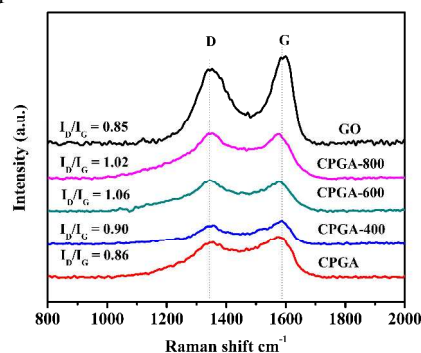


Fig. 2 Raman of as-prepared samples

Raman spectroscopy is one of the most useful methods to determine the defects, ordered and disordered structures, and the layers of graphene. As shown in Fig 2, all Raman spectra of GO and CPGAs have two prominent peaks at 1350 and 1600 cm⁻¹, which correspond to the D band arising from the disordered carbon atoms and the G band from sp²-hybridized graphitic carbon atoms²²⁻²³, respectively. In comparison, the I_D/I_G ratio of CPGAs (0.86 for CPGA, 0.83 for CPGA-400, 1.06 for CPGA-600 and 1.02 for CPGA-800) are slightly larger than that of GO (0.85), suggesting a broken hexagonal symmetry of graphene, most probably caused by either the heterogeneous N-dopants or the in-plane porosity of graphene²⁴. The crystallite size can be determined according to the Tuinstra–Koenig (TK) relation, $L_a(\text{nm}) = (2.4 \times 10^{-10}) \lambda^4 (I_D/I_G)^{-1}$ (λ is the Raman excitation wavelength)²⁵. According to calculation, the crystallite sizes for GO, CPGA, CPGA-400, CPGA-600 and CPGA-800 are 22.7, 22.3, 23.3, 18.1 and 18.9 nm, respectively. Considering L_a as the average interdefect distance, more defects undoubtedly means a smaller L_a ; Thus, CPGA-600 has much more defects than other samples.

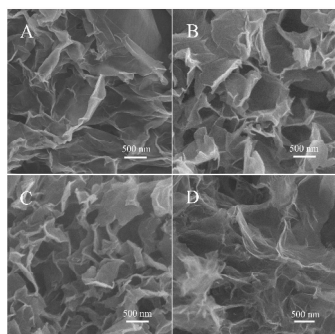


Fig. 3 SEM of as-prepared samples (A, CPGA; B, CPGA-400; C, CPGA-600; D, CPGA-800)

The microstructures of the as-prepared samples were investigated by SEM. As shown in Fig. 3, all of the samples display inter-connected 3D porous networks, which pore diameters ranged from submicrometer to several micrometers. It should be noted that the pore diameters of these samples become narrow with increasing the pyrolysis temperature, which may due to under high temperature graphite oxide (GO) lost some functional group to make graphene layers attracted each other. Further, when the pyrolysis temperature reaches to 800 °C, the obtained sheets get very thin, which may due to more carbonized PPy on the surface of GO is decomposed in high temperature annealing process.

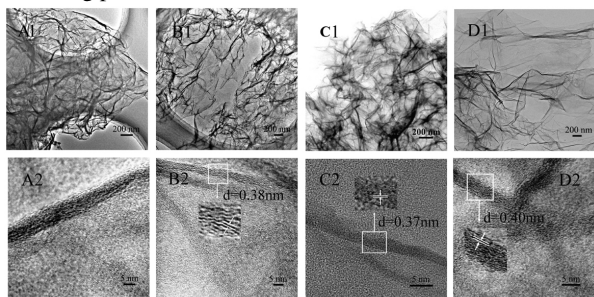


Fig. 4 TEM of as-prepared samples (A1 and A2, CPGA; B1 and B2, CPGA-400; C1 and C2, CPGA-600; D1 and D2, CPGA-800)

The microstructure of the as-prepared samples was further investigated by TEM. Fig.4 displays the typical nanosheets structure of these samples. The cross-sectional view of the suspended edge of the as-synthesized CPGAs (Figures 4 B2-D2) reveals that the graphene sheets are only a few layers (typically, 2-8 layers). Adjacent interlayer distances in the CPGAs film were 0.37~0.40 nm, which is close to the d-spacing of (002) crystal plane (0.335 nm) of bulk graphite with slight distortion²⁶. It can be seen clearly from these HRTEM images that the interlayer distance of outer sheets is evidently larger than that of inner sheets, which maybe is an evidence of the inhomogeneity carbonized PPy coated onto the graphene layers and hindered from the stacked together of graphene sheets.

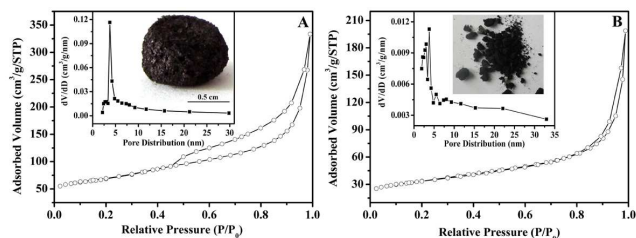


Fig. 5, BET of CPGA-600 and NG; the inset of Fig. 5 is the macroscopic structure of samples.

The microstructure of the resultant materials was further investigated by nitrogen adsorption–desorption experiments, as shown in Fig. 5. The nitrogen adsorption–desorption isotherms of NG and CPGA all exhibited mesoporous characteristics. Based on the N₂ adsorption experiment, the BET surface area of CPGA (231 m² g⁻¹) is obviously larger than that of NG (114 m² g⁻¹). The inset of Fig. 5 displays the macroscopic cylindrical structures of CPGA and powder of NG, combined the SEM and TEM observation, which suggests that the CPGA obtained in our work has well-developed 3D porous nanostructures and interconnected networks, which could provide fast ionic channels for electrochemical reaction.

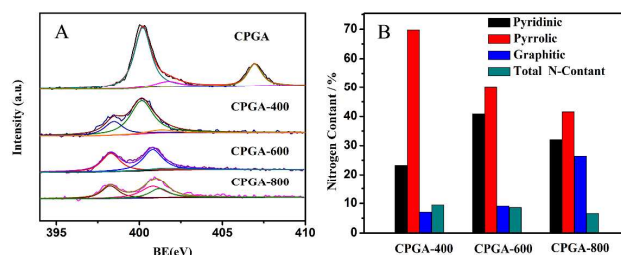


Fig. 6A High resolution N1s XPS spectra of CPGAs; 6B, the nitrogen content of CPGAs samples.

Figure 6A and B shows typical XPS spectra and the nitrogen content for CPGAs. N1s spectra of CPGAs were devoted to understand the different types of nitrogen in the samples (Fig. 6A). The N1s spectra of CPGA were deconvoluted into three different peaks at the binding energies of ~ 400.2, 401.7 and 406.9 eV²⁷, corresponding to pyrrolic N, graphitic N and oxide N²⁸. It indicated that under hydrothermal process part PPy formed order graphite structure containing N, which clearly supports that the presence of the carbonized PPy on the surface of the graphene sheets prior to annealing process, and the graphitic N and pyrrolic N of CPGA attributed to carbonized PPy. After annealing at three different temperatures, all the three samples are showing three different peaks corresponding to the pyridinic (398.3±0.2 eV), pyrrolic (400.8 eV) and graphitic (401.7±0.2 eV) nitrogen²⁹. With increasing annealing temperature, the graphitic nitrogen content of CPGAs progressively increases as shown in Fig.6B. In CPGA-800, the graphitic nitrogen content reached up to 26.4% compared to 9.1% obtained for NGA-600. However, the pyridinic nitrogen content shows non-line changes with annealing temperature increasing; highest pyridinic nitrogen of 40.9% was detected on CPGA-600. With the increasing of annealing temperature, the pyrrolic nitrogen content was decreased gradually. The results indicates that the PPy on the surface of graphene sheet

completely carbonized under higher temperature, most of the carbonized PPy formed orderly carbon nitride or N atoms of the carbonized PPy partly go into the skeleton of graphene sheet.

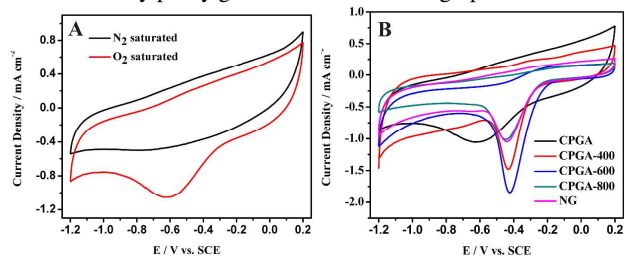


Fig. 7A, CV of CPGA in N_2 - and O_2 -saturated 0.1 M KOH aqueous solution at 50 mV s^{-1} ; **B**, CV of CPGAs and NG in O_2 -saturated 0.1 M KOH aqueous solution at 50 mV s^{-1}

We first examined the electrocatalytic properties of CPGA in N_2 -saturated and O_2 -saturated 0.1 M KOH aqueous solution using cyclic voltammetry at a scan rate of 50 mV s^{-1} . In Fig.7A, Featureless voltammetric currents within the potential range between -1.2 and +0.2 V were observed for CPGA in the N_2 -saturated solution, in contrast, when the electrolyte was saturated with O_2 , an obviously cathodic peak appeared at -0.62 V, which suggests CPGA has electrocatalytic activity for oxygen reduction. To investigate the effect of heat-treatment temperature on the performance of the as-prepared N-doped graphene aerogels, the electrocatalytic activity of CPGAs obtained at different annealing temperature and N-doped graphene (NG) prepared by conventional pyrolysis method toward the ORR process in oxygen saturated 0.1 M KOH aqueous solution was studied (Fig.7B). By comparing their CV curves, CPGA-600 shows the best activity with regard to the current density and overpotential (half-wave potential of -0.42 V, current density of 1.85 mA cm^{-2}). NG reveals lower current density and overpotential (half-wave potential of -0.44 V, current density of 0.93 mA cm^{-2}) than those of CPGA-600, which may be due to the interconnected porous network and conductive multiplexed pathways of CPGA-600 are beneficial to rapid ion diffusion and charge transfer and provides special reaction microenvironment for ORR. Recent the pyrrolic and pyridinic forms are reported to be the preferred coordinations of nitrogen due to their comparatively higher influence in reducing the overpotential for oxygen reduction³⁰. Our electrochemical results combined with XPS analysis indicated that pyrrolic-N and highly graphitized carbon structures are mainly responsible for the enhanced ORR activity of metal-free N doped carbon materials.

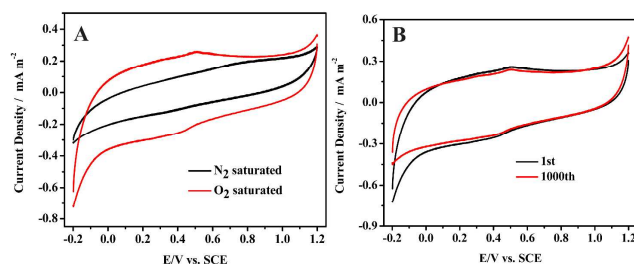


Fig. 8A, CV of CPGA-600 in N_2 - and O_2 -saturated 0.5 M H_2SO_4 aqueous solution at 50 mV s^{-1} ; **B**, CV of CPGA-600 in O_2 -saturated 0.5 M H_2SO_4 aqueous solution at 50 mV s^{-1} for 1st and 1000 cycles.

The ORR activity of CPGA-600 in acidic condition was also investigated by CV measurements. As shown in Fig.8A, There are obvious oxidation-reduction peaks for CPGA-600 in 0.5 M H_2SO_4 aqueous solution saturated with O_2 . However, comparing with its CV in O_2 -saturated 0.1 M KOH aqueous solution (Fig. 7B), the results indicated that the CPGA-600 is active catalysts for ORR in alkaline solution, whereas in acid media its electrocatalytic activity is very low. To further evaluate the stability of CPGA-600, we also compared the CV curves of the ORR for CPGA-600 before and after 1000 cycles in 0.5 M H_2SO_4 solution (Fig. 8B). There was no recordable loss of the current density decrease on CPGA-600 after 1000 cycles, which illustrates that the CPGA-600 is a highly stable catalyst for the ORR in an acidic medium.

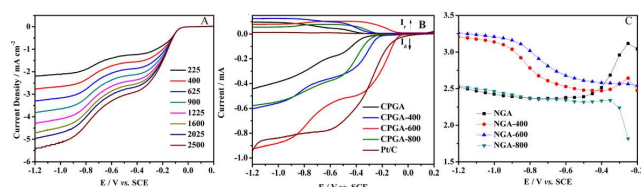


Fig. 9A, LSV of CPGA-600 in O_2 -saturated 0.1 M aqueous KOH solution at a scan rate of 10 mV s^{-1} at different RDE rotation rates (in rpm). **B**, RRDE test of the ORR on CPGAs and Pt/C in O_2 -saturated 0.1 M KOH aqueous solution at rotation rate of 1600 rpm. **C**, Electron transfer number of CPGA, CPGA-400, CPGA-600 and CPGA-800 as functions of the electrode potential.

Subsequently, to examine the reaction kinetics for CPGA-600 electrodes, linear sweep voltammograms (LSVs) were recorded in an O_2 -saturated 0.1M KOH electrolyte at a scan rate of 10 mV s^{-1} using a rotating disk electrode (RDE). The polarization curves of CPGA-600 at different potentials and rotation speeds are shown in Fig. 9A, two diffusion limiting current plateaus were observed, which means that a two-step reaction pathways take place on the surface of CPGA-600 electrode. Figure 9B shows the disk and ring currents for CPGAs and Pt/C in O_2 -saturated 0.1 M KOH aqueous solution at rotation rate of 1600 rpm. All four electrodes generated ring currents at the onset potential for the ORR. Notably, CPGA-600 exhibited much higher ring current than that of CPGA, CPGA-400 and CPGA-800 from -0.06 to -0.63 V, but the ring current of CPGA-600 decrease from -0.63 to -1.20 V. In terms of limiting current density, the highest value was obtained on CPGA-600, followed by CPGA-400, CPGA-800 and CPGA. For CPGA-400, CPGA-600, CPGA-800 and Pt/C, the onset potential was -0.32 V, -0.22 V, -0.06, -0.25 V and 0.01V, respectively. Clearly, the CPGA-600 electrode exhibits more positive onset potential in the CPGAs but not better than Pt/C. The positive shift of the onset potential and enhancement of the reduction current for ORR on the CPGA-600 electrode indicated that the CPGA-600 electrode possesses much higher electrocatalytic activity toward ORR than other CPGAs.

The electron transfer number (n) of the resulting different N-carbon materials was determined on the basis of the disk current (I_D) and ring current (I_R) via the following equation (1), where N is current collection efficiency of the Pt ring³¹.

$$n = \frac{4I_D}{(I_D + I_R/N)} \quad (1)$$

Figure 9c reveals that the electron transfer number varied strongly with the measured potential. The electron transfer numbers (n) were 2.5~3.1 for CPGA, 2.5~3.2 for CPGA-400, 2.6~3.3 for CPGA-600 and 1.8~2.5 for CPGA-800 over the potential range from -0.20 to -1.2 V, which indicated that the electrocatalytic process of CPGAs mainly via a four-electron mechanism. Combining the LSV results of CPGA-600 electrode, there should be taken place a two-electron and four-electron mixed mechanism, which may be due to the different catalytic active sites on the surface of CPGA-600.

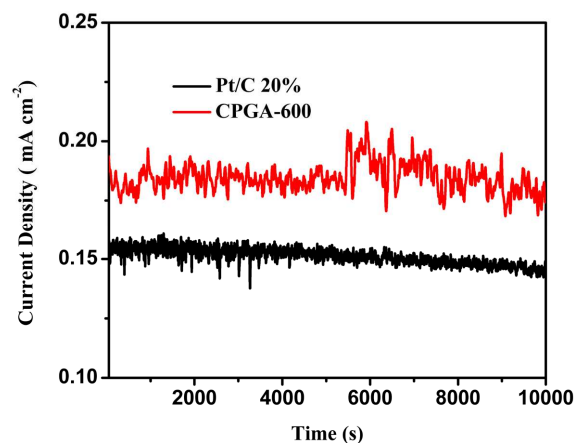


Fig. 10. I-t chronoamperometric responses of CPGA-600 and Pt/C electrode at -0.3 V in O_2 -saturated 0.1 M KOH solution

Fig. 10 shows current-time chronoamperometric results in 0.1 M KOH solution with continuous O_2 bubbling at -0.3 V (vs. SCE) for 10000 s. After 10000 s operation in severe alkaline media, Pt/C reveals significant performance degradation, indicating the poor stability of Pt/C in the alkaline environment. However, combined with the results of Fig. 8B, it is clearly that the CPGA-600 catalyst has high resistibility in alkaline and severe acidic environment.

4. Conclusion

In summary, a kind of carbonized PPy coated graphene aerogel was designed in this work. The effect of annealing temperature on the microstructure and electrochemical performance was also studied in detail. The experimental results indicated that the novel materials have well-developed porous nanostructures and interconnected networks, could provide fast ionic channels for electrochemical reaction. Although the resulting CPGA-600 displayed more negative onset potential than Pt/C toward ORR in alkaline media, the resulting CPGA-600 catalyst featured the almost four-electron transfer processes, high current density, and superb stability, potentially making it as a nonprecious metal catalyst for fuel cells and also has potential application in sensors, batteries, and supercapacitors.

Acknowledgments

The work is supported by grants from the National Natural Science Foundation of China (No. 21163021), Fundamental Research Funds for the Central Universities (XDJK2013B031),

the Natural Science Foundation of Chongqing (cstc2013jcyjA0396).

Notes and references

- ⁴⁵ *a* Key Laboratory of Material and Technology for Clean Energy, Ministry of Education, Key Laboratory of Advanced Functional Materials, Institute of Applied Chemistry, Xinjiang University, Urumqi 830046, Xinjiang Autonomous Region, P. R. China.
- b* Institute of Clean Energy & Advanced Materials, Southwest University, Chongqing, 400715, P.R. China. Fax: +86-023-68254969; Tel: +86-023-68254943. E-mail: baoshj@swu.edu.cn
- 1 D. Shin, B. Jeong, B. S. Mun, H. Jeon, H. J. Shin, J. Baik, and J. Lee, *J. Phys. Chem. C*, 2013, 117, 11619.
- 2 J. Lee, B. Jeong and J. D. Ocon, *Current Applied Physics*, 2013, 13, 309.
- 3 B. P. Vinayan and S. Ramaprabhu, *Nanoscale*, 2013, 5, 5109.
- 4 Z. C. Zuo, W. Li and A. M anthiram, *J. Mater. Chem. A*, 2013, 1, 10166.
- 5 C. Z. Zhu and S. J. Dong, *Nanoscale*, 2013, 5, 1753.
- 6 T. Fujigaya, T. Uchinoumi, K. Kaneko and N. Nakashima, *Chem. Commun.*, 2011, 47, 6843.
- 7 J. Liang, Y. Jiao, M. Jaroniec and S. Z. Qiao, *Angew. Chem*, 2012, 124, 1.
- 8 Z. Yang, H. G. Nie, X.A. Chen, X. H. Chen and S. M. Huang, *J. Power Sources*, 2013, 236, 238.
- 9 Z. H. Sheng, L. Shao, J. J. Chen, W. J. Bao, F. B. Wang and X. H. Xia, *ACS nano*, 2011, 5, 4350.
- 10 Y. F. Tang, B. L. Allen, D. R. Kauffman and A. Star, *J. Am. Chem. Soc.*, 2009, 131, 13200.
- 11, M. Cattelan, S. Agnoli, M. Favaro, D. Garoli, F. Romanato, M. Meneghetti, A.i Barinov, P. Dudin and G. Granozzi, *Chem. Mater.* 2013, 25, 1490.
- 12 Z. Liu, H. G. Nie, Z. Yang, J. Zhang, Z. P. Jin, Y. Q. Lu, Z. B. Xiao and S. M. Huang, *Nanoscale*, 2013, 5, 3283.
- 13 P. Huang, W. F. Chen and L. F. Yan, *Nanoscale*, 2013, 5, 6034.
- 14 Z. Y. Lin, G. H. Waller, Y. Liu, M. L. Liu, C. P. Wong, *Nano Energy* 2013, 2, 241 – 248.
- 15 L. Ren, K. S. Hui, and K. N. Hui, *J. Mater. Chem. A*, 2013, 1, 5689.
- 16 P. Chen, J. J. Yang, S. S. Li, Z. Wang, T. T. Xiao, Y. H. Qian, S. H. Yu, *Nano Energy*, 2013, 2, 249 – 256.
- 17 L. B. Zhang, G. Y. Chen, M. N. Hedhili, H. N. Zhang and P. Wang, *Nanoscale*, 2012, 4, 7038.
- 18 C. C. Ji, M. W. Xu, S. J. Bao, C. J. Cai, Z. J. Lu, H. Chai, F. Yang, and H. Wei, *J. Colloid Interface Sci.*, 2013, 407, 416.
- 19 C. J. Cai, M. W. Xu, S. J. Bao, C. Lei and D. Z. Jia, *RSC Adv.*, 2012, 2, 8172.
- 20 D. C. Marcano, D. V. Kosynkin, J. M. Berlin, A. Sinitiskii, Z. Z. Sun, A. Slesarev, B. Alemany, W. Lu and J. M. Tour, *ACS nano*, 2010, 4, 4807.
- 21 J. Liu, Z. Wang, Y. Zhao, H. H. Cheng, C. G. Hu, L. Jiang and L. T. Qu, *Nanoscale*, 2012, 4, 7563.
- 22 Z. J. Lu, S. J. Bao, Y. T. Gou, C. J. Cai, C. C. Ji, M. W. Xu, J. Song, R. Y. Wang, *RSC Adv.*, 2013, 3, 3990.
- 23 Z. J. Lu, M. W. Xu, S. J. Bao, K. Tan, H. Cai, C. J. Cai, C. C. Ji, Q. Zhang, *Acta Chim. Sinica*, 2013, 71, 957.
- 24 D. S. Yu, L. Wei, W. C. Jiang, H. Wang, B. Sun, Q. Zhang, K. L. Goh, R. Si and Y. Chen, *Nanoscale*, 2013, 5, 3457.
- 25 H. B. Wang, T. Maiyalagan, and X. Wang, *ACS Catal.* 2012, 2, 781.
- 26 L. T. Qu, Y. Liu, J. B. Baek, and L. M. Dai, *ACS nano*, 2010, 4, 1321.
- 27 R. Arrigo, M. Hävecker, S. Wrabetz, R. Blume, M. Lerch, J. McGregor, P. J. Parrott, J. A. Zeitler, L. F. Gladden, A. Knop-Gericke, R. Schlögl and D. S. Su, *J. Am. Chem. Soc.* 2010, 132, 9616.
- 28 Z. J. Lu, M. W. Xu, S. J. Bao, H. Cai, *J. Mater. Sci.* 2013, 48, 8101.
- 29 C. W. Tsai, M. H. Tu, C. J. Chen, T. F. Hung, R. S. Liu, W. R. Liu, M. Y. Lo, Y. M. Peng, L. Zhang, J. J. Zhang, D. S. Shy and X. K. Xing, *RSC Adv.*, 2011, 1, 1349.

-
- 30 S. M. Unni, S. Devulapally, N. Karjule and S. Kurungot, *J. Mater. Chem.*, 2012, 22, 23506.
- 31 Z. S. Wu, S. B. Yang, Y. Sun, K. Parvez, X. L. Feng and K. Müllen, *J. Am. Chem. Soc.* 2012, 134, 9082.

5